

# Interaction of antiproton with helium based on *ab-initio* calculations

Imre F. Barna<sup>1,2</sup>, Mihály A. Pocsai<sup>1,3</sup> and K. Tókési<sup>2,4</sup>

<sup>1</sup> *Wigner Research Center for Physics of the Hungarian Academy of Sciences Konkoly-Thege Miklós út 29 - 33,*

*1121 Budapest, Hungary* <sup>2</sup> *ELI-HU Nonprofit Kft.,*

*Dugonics Tér 13, H-6720 Szeged, Hungary* <sup>3</sup> *University of Pécs,*

*Institute of Physics, Ifjúság útja 6 H-7624 Pécs, Hungary,*

<sup>4</sup> *Institute of Nuclear Research of the Hungarian Academy of Sciences (ATOMKI),*

*H-4001 Debrecen, P.O. Box 51, Hungary*

(Dated: April 4, 2019)

## Abstract

We present ionization cross sections for antiproton and helium collisions based on *ab-initio* time-dependent coupled channel method. In our calculations a finite basis set of regular helium Coulomb wave packets and Slater function were used. The semiclassical approximation was applied with the time-dependent Coulomb potential to describe the antiproton electron interaction. Three different projectile energies were considered as 10, 50 and 100 keV. We found clear evidence for the formation of the anti-cusp in the differential distributions.

PACS numbers:

## I. INTRODUCTION

Collision between antiprotons and atoms has a fundamental interest in atomic physics. In the nineties numerous experimental and theoretical works were done with low energy antiprotons investigating various interesting phenomena [1]. Protons and antiprotons are the lightest heavy ions, where the semiclassical approximation is valid, therefore their motion can be treated classically. Contrast to protons at antiproton collisions—due to the negative charge—no electron transfer can take place which makes the electron dynamics much simpler at low energies.

In theoretical multi-electron atomic physics the investigation of antiproton helium collision has crucial interest.

There are three existing benchmark experiments where total cross ionization sections were measured for low energy collisions between antiprotons and helium atoms. The first two measurements were performed in 1990 [2] and 1994 [3]. More recently, single and double ionization cross sections of He and Ar atoms were investigated [4] by antiproton impact.

These experiments induced the “competition” between theories for the better and better descriptions of the physical processes, which is still very much active. In general, all theoretical descriptions predict almost the similar results above 100 keV antiproton collision energy, due to the weakening Sommerfeld parameter. This means that the interaction becomes perturbative and the first Born approximation is valid. The deviation between theory and experimental data becomes clearly visible between 10 and 100 keV impact energy and below 10 keV projectile energy, there are large deviations between non-perturbative *ab-initio* calculations. This is a clear indicator that the role of electron-electron correlation is crucial. However, until now, there has been no clear evidence of which theoretical model is superior. This paper now starts with a brief and non-exhaustive historical overview of the relevant existing theoretical models. The forced impulse method (FIM), developed by Reading and Ford [5] was one of the most successfully early method for proton and antiproton-helium collisions. An improved version of FIM is the multi-cut forced impulse (MFIM) method by [6]. Bent *et al.* [7] used multi-electron hidden crossing (MEHC) theory in their study of the single ionization of He in antiproton impact. The time-dependent density functional theory [8] is another powerful method to describe non-perturbative many-electron ionization processes, even in the low keV/amu impact energy range. Keim *et al.* [9] applied density

functional theory with various response functions and with a basis representation obtained from the basis generator method (BGM) to obtain single- and double-ionization cross sections in antiproton and helium collision systems. Later, the method was improved and the same scientific question was subsequently revised [10]. Single ionization of He antiproton impact was also studied by Tong *et al.* [11] using a self-interaction-free time-dependent density-functional theory (SIF-TDDFT).

Various independent particle close-coupling methods in a semi-classical impact parameter treatment, where the electron wave function is expanded around the target nucleus, are prominent among the theoretical studies [12–17].

Later, a fully correlated, three dimensional approach was developed by Schulz and Krstic [18] to study the ionization cross sections in collision between antiproton and helium atoms. They solved the time-dependent Schrödinger equation (TDSE) in a four dimensional Cartesian lattice (LTDSE) and calculated the ionization cross sections using  $75^4$  lattice points. The B-spline basis for the construction of the active electron wave function was used by Sahoo *et al.* [19]. B-splines have been widely used in atomic physics[20] because of their ability to accurately represent the continuum channels when compared with other conventional bases. Foster [21] published calculations obtained from lattice time dependent close coupling method.

Fainstein *et al.* [22] applied the Coulomb Distorted Wave Eikonal Initial State (CDW-EIS) method below 100 keV antiproton impact energies and had an astonishingly good agreement with experimental data of [3]. This induced a debate regarding the validity of CDW-EIS method.

The independent particle approach also has been performed by Schultz [23] using a classical trajectory Monte Carlo Method (CTMC).

First we applied a time dependent coupled channel (TDCC) method in a special basis for calculating the single ionization cross sections. Our results for angular differential ionization cross sections were compared with the results of CDW-EIS and CTMC methods [24]. Later also the energy and angular differential electron emission cross sections were presented using CDW-EIS and CTMC models [25].

In 2011, Kirchner and Knudsen published a topical review which exhaustively discussed and compared all the experimental results and theoretical model calculations [26].

In parallel to the development of theoretical ab-initio methods, there must also be a focus

on the deeper understanding of the dynamics of the anti-cusp dip, where the DDCSs have to be analyzed.

One of the interesting part of the collision physics is the study of electron emissions in the direction of the projectile motion. The electron capture to continuum (ECC) peak was discovered in 1970 by [27] in the double-differential cross section (DDCS) of electrons ejected in proton-atom collisions at 0 degree compared to the projectile initial velocity.

For positively charged particles, the production of the cusp peak is experimentally and theoretically understood [28]. Numerous investigations lead to the conclusion that the cusp is generated when the asymptotic velocity of the ionized electron is equal with the velocity of the projectile.

It can be explained for positively charged projectiles as result of the special case of ionization, where the ionized target electron is strongly influenced by the outgoing projectile, or in other words when the atomic electron is dragged by the projectile continuum state and moves with it. Following this scenario, using the negatively charged projectiles we can expect electron yield deficit in the direction of the projectile path and we can expect anti-cusp formation instead of cusp formation.

However, for negative charged projectile impact, due to the very limited available experimental data, the production of the anti-cusp is barely understood, especially at low impact energies. The anti-cusp supposes that a well defined gap must exist in the energy spectrum of the ionized electron in the direction of the projectile. Numerous theoretical studies have addressed the question of anti-cusp from different authors [29–34]. To the best of our knowledge, only the total ionization cross section data is so-far available from experiments and there are no available *ab initio* calculations for differential ionization cross sections for antiproton helium impact.

In this work we present ionization cross sections for antiproton and helium collisions based on *ab-initio* time-dependent coupled channel method. In our calculations a finite basis set of regular helium Coulomb wave packets and Slater functions are used. We show results for singly- and doubly differential cross sections at 10, 50 and 100 keV antiproton impact energies. So we believe, that this study might stimulate experimentalists to investigate this problem in the low energy antiproton-atom collisions in the future.

This paper contains a brief outline the used theoretical approach (Section 2) with the calculated results are presented and discussed in Section 3. Atomic units are used throughout

the paper unless otherwise indicated.

## II. THEORY

The TDCC method has been widely used in various fields of atomic collision physics with the recognition that it is one of the most reliable and powerful theoretical approaches [26]. Our single-center coupled-channel method was first introduced for the ionization of helium in relativistic heavy ion collisions [35, 36]. Later, the same model was applied for positron helium collisions [37]; for the photoionization [38] and finally for two-photon double-ionization of helium [39]. Currently, a very similar model is used to investigate photoionization of rubidium atoms [40].

In the semi-classical approximation, the projectile moves on a straight-line trajectory, with constant velocity  $v$  and impact parameter  $b$ . The projectiles are considered to be classical point charges without any inner structure.

To study the ionization process, the time-dependent Schrödinger equation is solved with a time-dependent external Coulomb field:

$$i\frac{\partial}{\partial t}\Psi(\mathbf{r}_1, \mathbf{r}_2, t) = \left(\hat{H}_{He} + \hat{V}(t)\right)\Psi(\mathbf{r}_1, \mathbf{r}_2, t), \quad (1)$$

where  $\hat{H}_{He}$  is the Hamiltonian of the unperturbed helium atom

$$\hat{H}_{He} = \frac{p_1^2}{2} + \frac{p_2^2}{2} - \frac{2}{r_1} - \frac{2}{r_2} + \frac{1}{|\mathbf{r}_1 - \mathbf{r}_2|}. \quad (2)$$

The external time-dependent field  $\hat{V}(t)$  is the antiproton-electron interaction

$$\hat{V}(t) = -\left(\frac{1}{R_1(t)} + \frac{1}{R_2(t)}\right) \quad (3)$$

with  $R_i(t) = ((x_i - b)^2 + y_i^2 + (z_i - v_p t)^2)^{1/2}$ ,  $i = 1, 2$ . Below 20 keV, impact energies instead of the straight-line trajectories Coulomb hyperbolas are used. For collision energies below 1keV, the trajectory bending effect is even more important. Originally the retarded Lenard-Wiéchert potentials were used for relativistic collisions [35]. Eq. (1) is solved by the expansion of  $\Psi(\mathbf{r}_1, \mathbf{r}_2)$  in the basis of eigenfunctions  $\{\Phi_j\}$  of the time-independent Schrödinger equation:

$$\hat{H}_{He}\Phi_j(\mathbf{r}_1, \mathbf{r}_2) = E_j\Phi_j(\mathbf{r}_1, \mathbf{r}_2), \quad (4)$$

with

$$\Psi(\mathbf{r}_1, \mathbf{r}_2, t) = \sum_{j=1}^N a_j(t) \Phi_j(\mathbf{r}_1, \mathbf{r}_2) e^{-iE_j t}, \quad (5)$$

where  $a_j(t)$  are the time-dependent expansion coefficients for the various channels described by the wave functions  $\Phi_j$ . Inserting this Ansatz into Eq. (1) leads to a system of first-order differential equations for the expansion coefficients:

$$\frac{da_k(t)}{dt} = -i \sum_{j=1}^N V_{kj}(t) a_j(t) e^{i(E_k - E_j)t}, \quad (k = 1, \dots, N), \quad (6)$$

where  $V_{kj}$  is the coupling matrix  $\langle \Phi_k(\mathbf{r}_1, \mathbf{r}_2) | \hat{V}(t) | \Phi_j(\mathbf{r}_1, \mathbf{r}_2) \rangle$  including the symmetrized products of the projectile-electron single-particle interaction matrix elements and electron-electron single-particle overlap matrix elements, respectively.

Denoting the ground state with  $k = 1$ , the following initial conditions are used

$$a_k(t \rightarrow -\infty) = \begin{cases} 1 & \text{for } k = 1, \\ 0 & \text{for } k \neq 1. \end{cases} \quad (7)$$

The total cross section for occupying the helium eigenstate  $k$  can be calculated as

$$\sigma_k = \int P_k(\mathbf{b}, t \rightarrow \infty) d^2b, \quad (8)$$

with the probability

$$P_k(\mathbf{b}, t \rightarrow \infty) = |a_k(t \rightarrow \infty)|^2. \quad (9)$$

The coupled system of Eq. (6) is solved numerically by using a Runge-Kutta-Fehlberg method of fifth order with embedded automatic time step regulation. The conservation of the norm of the wave function is fulfilled better than  $10^{-8}$  during the collision.

The eigenfunctions  $\Phi_j$  in Eq. (4) are obtained by diagonalizing the Hamiltonian in a basis of orthogonal symmetrized two-particle functions  $f_\mu$  so that

$$\Phi_j(\mathbf{r}_1, \mathbf{r}_2) = \sum_{\mu} b_{\mu}^{[j]} f_{\mu}(\mathbf{r}_1, \mathbf{r}_2). \quad (10)$$

In the applied independent particle model the many-particle wave functions  $f_\mu$  are built up from single-particle orbitals. For these single-particle wave functions, an angular momentum representation with spherical harmonics  $Y_{l,m}$ , hydrogen-like radial Slater functions and radial regular Coulomb wave packets is used. The Slater function can be written

$$S_{n,l,m,\kappa}(\mathbf{r}) = c(n, \kappa) r^{n-1} e^{-\kappa r} Y_{l,m}(\theta, \varphi), \quad (11)$$

where  $c(n, \kappa)$  is the normalization constant. A regular Coulomb wave packet

$$C_{k,l,m,Z}(\mathbf{r}) = q(k, \Delta k) Y_{l,m}(\theta, \varphi) \int_{E_k - \Delta E_k/2}^{E_k + \Delta E_k/2} F_{k,l,Z}(r) dk \quad (12)$$

with normalization constant  $q(k, \Delta k)$  is constructed from the radial Coulomb function

$$F_{k,l,Z}(r) = \sqrt{\frac{2k}{\pi}} e^{\frac{\pi\eta}{2}} \frac{(2\rho)^l}{(2l+1)!} e^{-i\rho} |\Gamma(l+1-i\eta)| \times {}_1F_1(1+l+i\eta, 2l+2, 2i\rho), \quad (13)$$

where  $\eta = Z/k$ ,  $\rho = kr$ .

The wave packets cover a small energy interval  $\Delta E_k$  and thereby forms a discrete representation of the continuum which can be incorporated into the finite basis set. The normalized Coulomb wave packets are calculated up to more than 300 a.u. radial distance to achieve a deviation of less than one percent from unity in their norm.

In this approach, two different effective charges  $Z$  for the target nucleus have been used to take into account the difference between the the singular and the double ionized stats of the He atoms. For single-ionized states,  $Z = 1$  and for the double-ionized case  $Z = 2$  were used, respectively.

The single- and double-continuum electron sates were calculated up to 6 a.u. energy equidistantly.

We include single-particle wave functions with  $0 \leq l_1, l_2 \leq 2$  angular momenta and couple them to  $0 \leq L \leq 2$  total angular momentum two-electron states. For the  $L = 0$  configurations we use ss+pp+dd angular correlated wave functions, for  $L = 1$  we use sp+pd couplings and for  $L = 2$  the sd+pp+dd configurations, respectively. For the ground state energy of He (1s1s) the -2.901 a.u. was obtained which is reasonably accurate compared to the “exact” value of -2.903 a.u.

The diagonalization process gives 465 basis states which correspond to 1490 different collision channels, including different  $m_l$  sub-states. The highest energy eigenvalue lies at 27.8 a.u. Numerous different basis sets were applied in order to test for convergence of the expansion (5). The results demonstrate that the channels with energies above 5 a.u contribute very little to the ionization probabilities. The basis between the first ionization threshold (-2.0 a.u.) and the lowest auto-ionizing quasi-bound state ( “2s2s” E = -0.77 a.u. L=0), contained 22 discretized continuum states per total angular momenta, providing the major contribution for single-ionization.

The Feshbach projection [35] together with the complex scaling were adopted in order to separate excitation, double- and single-ionization cross sections. In the first step, a new “reference” Hilbert subspace was constructed and split into three different orthogonal subspaces characterized by the properties of the two electrons: 1 - bound-bound, 2 - bound-ionized and 3 - ionized-ionized electrons, respectively. In the second step, the “calculated Hilbert” space was projected onto the reference space and this determined the excitation, single- and double-ionization contributions. To fix the effective charge of the Coulomb wave function used in the helium wave functions, the excitation and single-ionization cross sections were compared with the results obtained from the complex scaling [38]. Doubly-excited states embedded in the continuum e.g., “2s2s” (this labeling should not be taken literally because of the strong electron-electron correlation [41]), can be identified by the method of complex scaling and therefore the double-excitation and the single-ionization states can be separated. This new combination of the two methods is still not exactly rigorous but is much more feasible than the Feshbach method alone and therefore reduces ambiguity.

To calculate the angular-differential ionization cross sections, the density operator was taken. The electron final-state density can be determined from the time-dependent wave function after the collision ( $t \rightarrow \infty$ ) according to the expectation value of the density operator  $\hat{\rho} = \sum_{i=1,2} \delta(\mathbf{r} - \mathbf{r}_i)$  for a fixed impact parameter  $\mathbf{b}$

$$\rho_{\mathbf{b}}(\mathbf{r}) = \left\langle \Psi(\mathbf{r}_1, \mathbf{r}_2) \left| \sum_{i=1,2} \delta(\mathbf{r} - \mathbf{r}_i) \right| \Psi(\mathbf{r}_1, \mathbf{r}_2) \right\rangle. \quad (14)$$

In order to extract the angular distribution of the ionized electrons two additional operations are needed:

1. The wave function  $\Psi$  is projected onto the single-ionization continuum  $|\Psi_{ion}\rangle = (1 - \hat{P}_b - \hat{P}_{di}) |\Psi\rangle$  where  $\hat{P}_b$  is the projector onto the bound state subspace (including all excited states) and  $\hat{P}_{di}$  is the projector onto double-ionized states.
2. The radial and the azimuthal coordinates have to be integrated over to get the polar angle distribution of the ionized electrons:

$$P_{\mathbf{b}}(\theta) = \frac{1}{2\pi} \int_0^{2\pi} \int_0^{\infty} \langle \Psi_{ion} | \sum_{i=1,2} \delta(\mathbf{r} - \mathbf{r}_i) | \Psi_{ion} \rangle r^2 dr d\varphi =$$

$$\frac{1}{\pi} \int_0^{2\pi} \int_0^{\infty} \int_{\mathbf{r}_1} |\Psi_{ion}|^2 d^3r_1 r^2 dr d\varphi. \quad (15)$$

The angular differential cross section is obtained by integrating  $P_b(\theta)$  over the impact parameter. This method has already been used in a previous publication [24] and it gives a satisfactory agreement with other theoretical results.

Contrary to other perturbative or classical approaches, TDCC methods has a finite number of discretized final-states. This is why it is not possible to calculate energy-differential cross sections in a rigorous way – only the distribution of the channel cross sections divided by an effective energy can be obtained. This effective energy can be defined in different ways, it can be the energy of the corresponding channel; the difference of the energies of the neighboring two channels or the widths of the Coulomb wave packets (12). Here we consider the last one, and we use the form for calculating the approximated energy differential cross sections according to the following equation:

$$\frac{d\sigma}{dE} \approx \frac{\sigma_k}{\Delta E_k}. \quad (16)$$

### III. RESULTS AND DISCUSSIONS

Table 1 shows our recent total single-ionization cross sections with some of the latest theoretical data. Figs. 1a, 2a, 3a display the DDCS for single ionization of helium at 10, 50 and 100 keV antiproton impact energies within the framework of the TDCC method. According to the figures, generally, we can conclude the followings: In each cases we found a minimum at zero angle indicating the existence of the Coulomb hole (“anti-cusp”). In general we can say, that the anti-cusps are always properly appear with antiproton projectile impact. As the projectile energy enhances the centers of the anti-cusps enhance too. At 10 keV the DDCS are generally smaller than for 50 or 100 keV. Despite the numerous theoretical studies investigations into the anti-cusp [31, 42, 43] over the last decades, there is still no experimental observation of the anti-cusp in anti-proton impacts. Slow electrons are possibly ejected into the backward direction and the fast electrons are ejected along the broad ridge identified as the binary encounter (BE) ridge. This BE ridge may be the easiest feature to understand as fast electrons are ejected through a series of hard collisions between the projectile and the target known as the Fermi-shuttle mechanism [44]. For all

Energy [keV ]	$\sigma^+$ (our)	$\sigma^+$ [21]	$\sigma^+$ [10]
10	0.45	0.43	0.48
50	0.58	0.62	0.63
100	0.61	0.60	0.68

TABLE I: Single-ionization cross sections ( $\sigma^+$ ) for the investigated energies. The second column presents our results, the third one is from [21] and the fourth one is from [10]. All numerical values should be multiplied by  $10^{-16}\text{cm}^2$ .

three energies (10, 50 and 100 keV), the ridge follows closely this trend.

The distribution of slow electrons in backward directions is a clear indication of final state interactions between the ejected electron and the antiproton. As the force between the electron and the anti-proton is repulsive, slow electrons ( $v_e < v_p$ , where  $v_e$  and  $v_p$  are the electron and projectile speeds, respectively) lag behind the antiproton and will be scattered to the backward direction. For the total cross section the contribution of slow electrons is dominated therefore the angular distribution in the DDCS will be suppressed in the forward direction, as clearly shown in Fig. 1a, 2a and 3a. This is in sharp contrast to proton impact, where single differential cross sections will generally peak at small angles and decrease toward large angles. The remarkable contrast to proton impact is the anti-cusp (void) region for anti-proton impact. This can also be attributed to the repulsive final state interactions.

To have a more transparent overview of the trends of our calculations we show additional figures, namely cuts at constant energies and cuts at constant scattering angles for all the three energies.

Figure 1b shows the energy differential cross sections at given angles. The cuts are parallel to the x (or energy) axis at 0, 60 and 120 degrees which are at the cusp, at the ridge and above the ridge. The presence of the anti-cusp is evident. At low electron energies, (around the ionization threshold) the cross sections are 10000 times lower for 20 degree emission angle than for 60 degree emission angle. Note that a factor of 100 remains even at 70 eV electron energies. The ratio of the cross sections between 60 and 120 degrees are much smaller.

Fig. 1c shows the angular differential cross sections at 20, 40 and 60 eV energies. We note that at zero scattering angle the electrons with 20 eV kinetic energy have a 10000

times smaller cross section than the electrons with energy of 40 eV.

Fig. 2a shows the DDCS for 50 keV antiproton impact energy. The general features remain the same—however, all differential cross sections are larger in accordance with the total cross sections. The position of the anti-cusp lies at 30 eV. On the contrary the maximal widths of the corresponding anti-cusp angle is reduced from 20 degrees to 5. Fig. 2b shows the cross sections at different emission angles. Note, that the cross sections lie in almost the same magnitude in all directions. This is drastically different to the 10 keV energy case. Fig. 2c shows the angular distributions for 20 and 40 eV energy electrons. Here again at zero scattering angle the electrons with 20 eV kinetic energy have a 10000 times smaller cross sections than the electrons with energy of 40 eV

Figure 3 shows the ionisation cross sections for 100 keV antiproton with the same general features. The center of the anti-cusp is at 50 eV with the energy widths of  $\pm 30$  eVs. It is clear to see in Fig. 3b that at zero emission angle and at backscattering all the three cross sections lie in almost the same magnitude. Fig. 3c shows a significant difference to Fig. 2c and Fig. 1c in that the cross section curves does not cross—a clear fingerprint that the whole distribution has become much more flat.

#### IV. SUMMARY AND CONCLUSIONS

The singly and doubly differential ionization cross sections for antiproton and helium atom collisions at 10, 50 and 100 keV impact energies were presented. The calculations were based on *ab-initio* time-dependent coupled channel method using a finite basis set of regular helium Coulomb wave packets and Slater function. A semiclassical approximation was applied with the time-dependent Coulomb potential to describe the antiproton electron interaction. We found a strong final state interactions between the antiprotons and the ejected electrons in the forward scattering angles. We clearly identified the existence of the formation of anti-cusp for each antiproton impacts. We hope that our recent calculations will further encourage the experimentalist to carry out differential cross section measurements in the in the near future.

10 keV  $p^- + \text{He}$

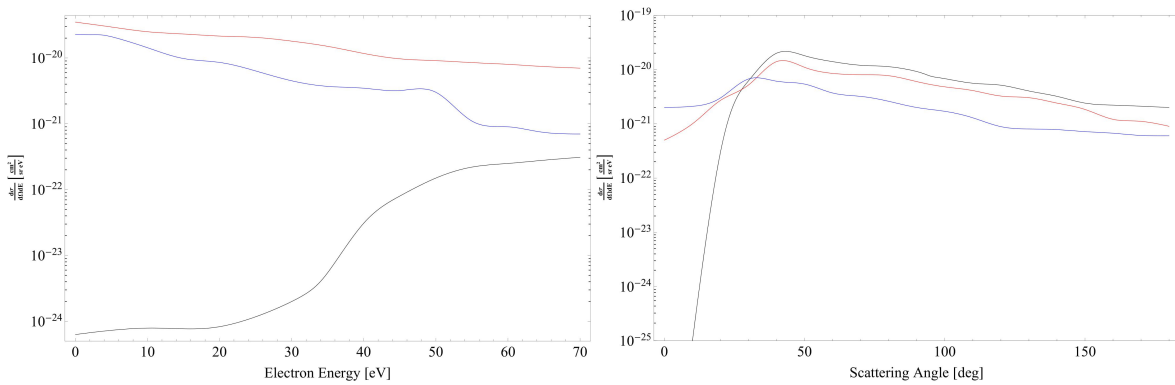
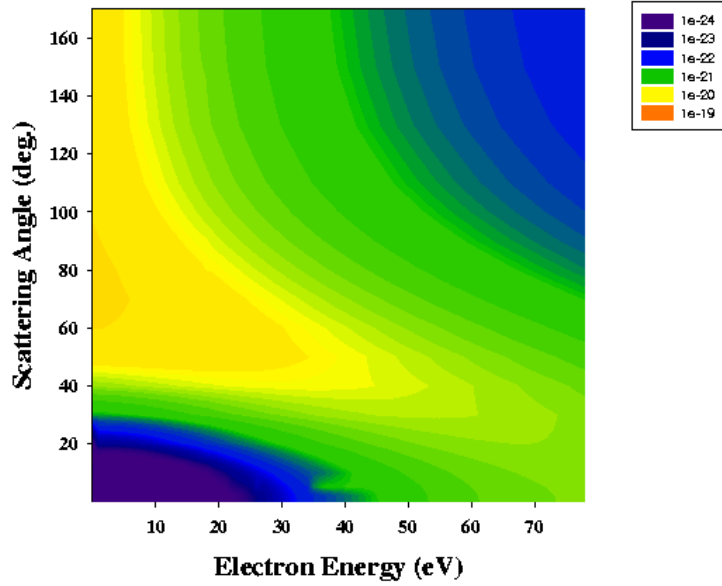


FIG. 1: a) Doubly differential electron emission cross sections emitted from He and 10 keV antiproton impact.

b) Three cuts of the DDCS at different angles. The black line is for 0, the red line is for 60 and the blue one is for 120 degrees.

c) Three cuts of the DDCS at different energies. The black line is for 20, the red line is for 40 and the blue one is for 60 eV.

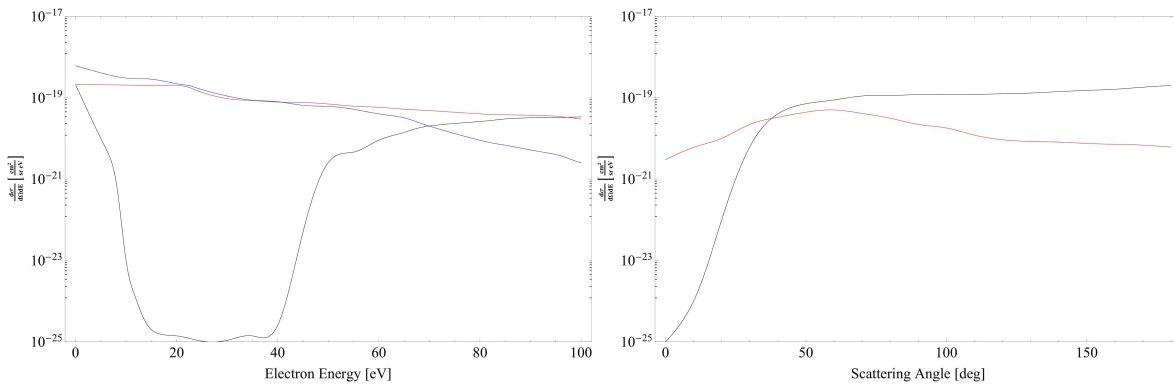
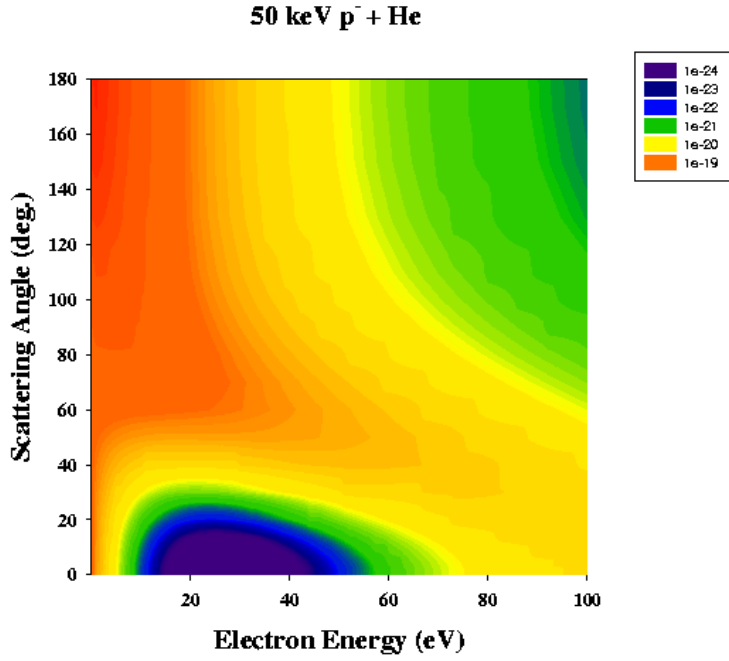


FIG. 2: a) The same as Fig. 1 but for 50 keV impact energy.

b) Three cuts of the DDCS at different angles. The black line is for 0, the red line is for 60 and the blue one is for 120 degrees.

c) Two cuts of the DDCS at different energies. The black line is for 20, the red line is for 40 eV.

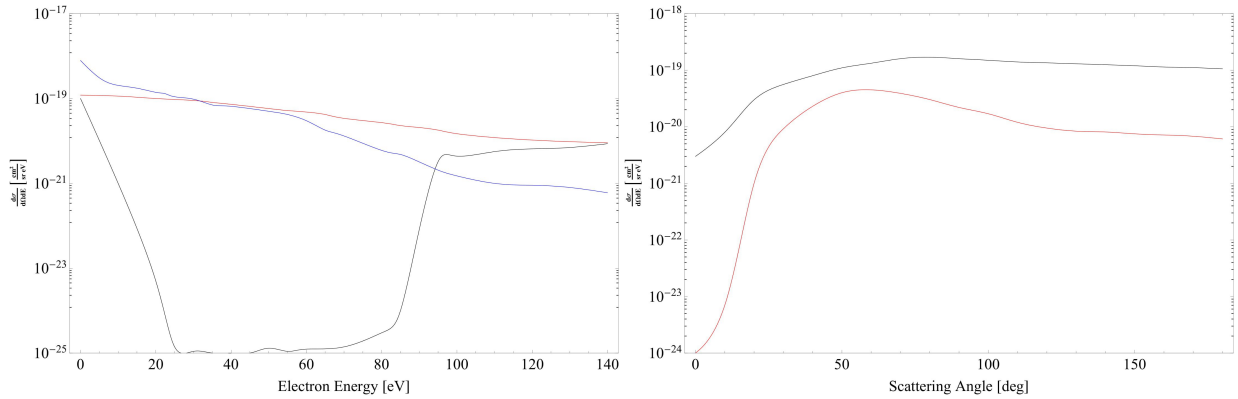
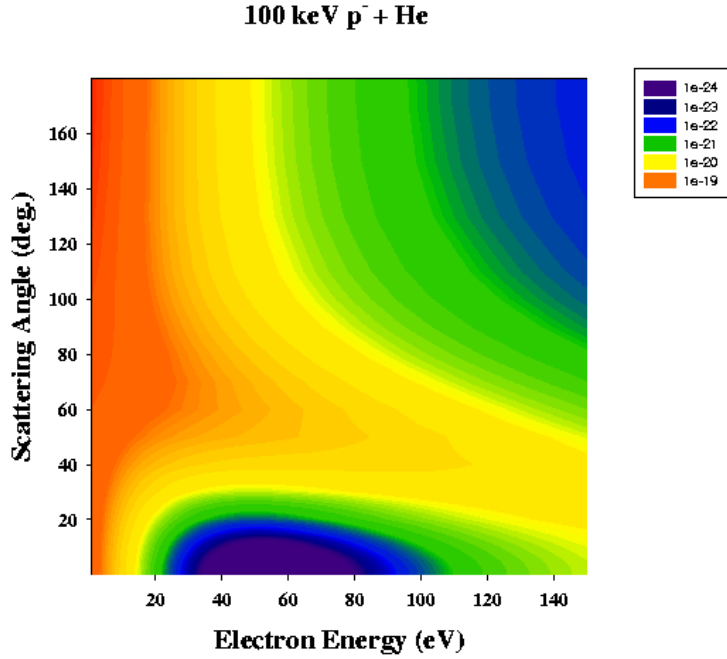


FIG. 3: a) The same as Fig. 1 but for 100 keV impact energy.

b) Three cuts of the DDCS at different energies. The black line is for 30, the blue is for 60 and the red one is for 120 degrees.

c) Two cuts of the DDCS at different energies. The black line is for 20, the red line is for 40 eV.

## V. ACKNOWLEDGMENTS

We would like to thank Dr. Andrew Cheesman for the critical reading of the manuscript. The ELI-ALPS project (GINOP-2.3.6-15-2015-00001) is supported by the European Union and co-financed by the European Regional Development Fund. One of us (KT) was also supported by the National Research, Development and Innovation Office (NKFIH) Grant KH126886, and by the European Cost Actions CA15107 (MultiComp).

- 
- [1] *International Workshop on Atomic Collisions and Atomic Spectroscopy with Slow Antiproton*, Book of Abstracts July 19-21, 1999 Tsurumi, Yokohama, Kanagawa, Japan, <http://radphys4.c.u-tokyo.ac.jp/pbar99/AbstractFinal3.pdf>
  - [2] L.H. Andersen, P. Hvelplund, H. Knudsen, S.P. Moller, J.O.P. Pedersen, S. Tang-Petersen, E. Uggerhoj, K. Elsner and E. Morenzoni, *Phys. Rev. A* **40**, (1990) 7366.
  - [3] P. Hvelplund, H. Knudsen, U. Mikkelsen, E. Morenzoni, S.P. Moller, E. Uggerhoj and T. Worm, *J. Phys. B* **27**, (1994) 925.
  - [4] H. Knudsen, H.-P. E. Kristiansen, H. D. Thomsen, U. I. Uggerhoj, T. Ichioka, S. P. Moller, C. A. Hunniford, R.W. Mullough, M. Charlton, N. Kuroda, Y. Nagata, H. A. Torii, Y. Yamazaki, H. Imao, H. H. Andersen, and Tókési *Phys. Rev. Lett.* **101**, (2008) 043201.
  - [5] A.L. Ford and J.F. Reading, *J. Phys. B* **27**, (1994) 4215.
  - [6] J.F. Reading, T. Bronk, A.L. Ford, L. Wherman and K.A. Hall, *J. Phys. B* **30**, (1997) L189.
  - [7] G. Bent, P.S. Krstic and D.R. Schultz, *J. Chem. Phys.* **108**, (1998) 1459.
  - [8] H.J. Lüdde, T. Kirchner and M. Horbatsch, *Quantum mechanical treatment of ion collisions with many-electron atoms*, in: *Photonic, Electronic, and Atomic Collisions*, ed. by J. Burgdörfer *et al.*, Rinton Press, Princeton, p. 708.
  - [9] M. Keim, A. Achenbach, H.J. Lüdde and T. Kirchner, *Phys. Rev. A* **67**, (2003) 062711.
  - [10] N. Henkel, M. Keim, H.J. Lüdde and T. Kirchner, *Phys. Rev. A* **80**, (2003) 032704.
  - [11] X-M. Tong, T. Watanabe, D. Kato and S. Ohtani, *Phys. Rev. A* **66**, (2002) 032709.
  - [12] G. Schiwietz, U. Wille, R.D. Muino, P.D. Fainstein and P.L. Grande, *J. Phys. B* **29**, (1996) 307.
  - [13] L.A. Wherman, A. L. Ford and J.F. Reading, *J. Phys. B* **29**, (1996) 5831.

- [14] A. Igarashi, A. Ohsaki and S. Nakazaki, Phys. Rev. A **62**, (2000) 052722.
- [15] C.Díaz, F. Martin and A. Salin, J. Phys. B **35**, (2002) 2555.
- [16] T.G. Lee, H.C. Tseng and C.D. Lin, Phys. Rev. A **61**, (2000) 062713.
- [17] M.S. Pindzola, T.G. Lee and J. Colgan, J. Phys. B. At. Mol. Opt. Phys. **44**, (2011) 205204.
- [18] D.R. Schulz, and P.S. Krstic, Phys. Rev. A **67**, (2003) 022712.
- [19] S. Sahoo, S.C. Mukherjee and H.R.J. Walters, J. Phys. B **37**, (2004) 3227.
- [20] F. Martin, J. Phys. B: At. Mol. Opt. Phys. **32**, (1999) R197.
- [21] M. Foster and J. Colgan and M.S. Pindzola, Phys. Rev. Lett. **100**, (2008) 033201.
- [22] P.D. Fainstein, V.H. Ponce and R.D. Rivarola, Phys. Rev. A **36**, (1987) 3639.
- [23] D.R. Schultz, Phys. Rev. A **40**, (1989) 2330.
- [24] I.F. Barna, L. Gulyás, K. Tókési and J. Burgdörfer, Rad. Phys. and Chem. **76**, (2007) 495.
- [25] K. Tókési, J. Wang, L. Gulyás, and J. Burgdörfer, Hyperfine Interaction, **194**, (2009) 45.
- [26] T. Kirchner and H. Knudsen, J. Phys. B. At. Mol. Opt. Phys. **44**, (2011) 122001.
- [27] G.B. Crooks and M.E. Rudd, Phys. Rev. Lett. **25**, (1970) 1599.
- [28] N. Stolterfoht, R.D. DuBois and R.D. Rivarola, *Electron Emission in Heavy Ion-Atom Collisions*, Springer, Berlin 1997.
- [29] C.O. Reinhold and J. Burgdörfer, J. Phys. B **26**, (1993) 3101.
- [30] Y. Yamazuki, K. Kuroki, K. Komaki, L.H. Andersen, E. Horsdal-Pettersen, P. Hvelplund, H. Knudsen, S.P. Moller, E. Uggerhoj and K. Elsner, Journal of the Physical Society of Japan **59**, (1990) 2643.
- [31] J. Burgdörfer, J. Wang and J. Müller, Phys. Rev. Lett. **62**, (1989) 1599.
- [32] P.D. Fainstein, V.H. Ponce and R.D. Rivarola, J. Phys. B. **21**, (1988) 2989.
- [33] R.E. Olson and T.J. Gay, Phys. Rev. Lett. **61**, (1988) 302.
- [34] C.O. Reinhold and R.E. Olson, Phys. Rev. A **39**, (1989) 3861.
- [35] I.F. Barna, N. Grün and W. Scheid, Eur. Phys. J. D. **25**, (2003) 239.
- [36] I.F. Barna, *Ionization of helium in relativistic heavy-ion collisions*  
 Doctoral thesis, University Gießen (2002), “Giessener Elektronische Bibliothek”  
<http://geb.uni-giessen.de/geb/volltexte/2003/1036>.
- [37] I.F. Barna, Eur. Phys. J. D **30**, (2004) 5.
- [38] I.F. Barna and J.M. Rost, Eur. Phys. J. D **27**, (2003) 287.
- [39] I.F. Barna, K. Tókési and J. Burgdörfer, J. Phys. B **38**, (2005) 1001.

- [40] M.A Pocsai, I.F. Barna and K. Tókési, *in print in EPJD*.
- [41] Y.K. Ho, Phys. Rev. A **34**, (1986) 4402.
- [42] R.E. Olson and T.J. Gay, Phys. Rev. Lett. **61**, (1998) 302.
- [43] C.O. Reinhold and J. Burgdörfer, J. Phys. B **26**, (1993) 3101.
- [44] B. Sulik, Cs. Koncz, K. Tókési, A. Orbán and D. Berényi, Phys. Rev. Lett. **88**, (2002) 073201.